Surface Nanodeformations Caused by Ultrashort Laser Pulse

N.A. Inogamov[1,a], V.V. Zhakhovsky[2,3,b], S.I. Ashitkov[3,c], Yu.N. Eminov[4,d], A.Ya. Faenov[3,e], Yu.V. Petrov[1,f], V.A. Khokhlov[1,g], M. Ishino[5,h], B.J. Demaske[2,i], M. Tanaka[5,j], N. Hasegawa[5,k], M. Nishikino[5,l], S. Tamotsu[6,m], T.A. Pikuz[3,5,n], I.Y. Skobelev[3,o], T. Ohba[5,p], T. Kaihori[5,q], Y. Ochi[5,r], T. Imazono[5,s], Y. Fukuda[5,t], M. Kando[5,u], Y. Kato[7,v], T. Kawachi[5,w], S.I. Anisimov[1,x], M.B. Agranat[3,y], I.I. Oleynik[2,z], and V.E. Fortov[3,zz]

[1] Landau Institute for Theoretical Physics, Russian Academy of Sciences, Chernogolovka, Moscow region, 142432, Russian Federation

[2] Department of Physics, University of South Florida, Tampa, Florida 33620, USA

[3] Joint Institute for High Temperatures, Russian Academy of Sciences, Moscow, 125412, Russian Federation

[4] Nanomaterials and Nanomanufacturing Research Center, University of South Florida, Tampa, Florida 33620, USA

[5] Quantum Beam Science Directorate, JAEA, Kizugawa, Kyoto 619-0215, Japan

[6] Graduate School of Humanities and Science, Nara Women's University, Nara 630-8506, Japan

[7] Graduate School for the Creation of New Photonics Industries, Hamamatsu,431-1202, Japan

[a] nailinogamov@gmail.com, [b] vasily@usf.edu, [c] Ashitkov11@yandex.ru, [d] emirov@usf.edu, [e] anatolyf@hotmail.com, [f] uvp49@mail.ru, [g] v_a_kh@mail.ru, [h] ishino.masahiko@jaea.go.jp, [i] bdemaske@mail.usf.edu, [j] Momoko.Tanaka@jaea.go.jp, [k] Noboru.Hasegawa@jaea.go.jp, [l] Masaharu.Nishikino@jaea.go.jp, [m] tamotsu@cc.nara-wu.ac.jp, [n] tapikuz@mail.ru, [o] skobelev@ihed.ras.ru, [p] Toshiyuki.Ohba@jaea.go.jp, [q] Takeshi.Kaihori@jaea.go.jp, [r] Yoshihiro.Ochi@jaea.go.jp, [s] Takashi.Imazono@jaea.go.jp, [t] fukuda.yuji@jaea.go.jp, [u] kando.masaki@jaea.go.jp, [v] y.kato@gpi.ac.jp, [w] Tetsuya.Kawachi@jaea.go.jp, [x] anisimov@itp.ac.ru, [y] agranat2004@mail.ru, [z] oleynik@usf.edu, [zz] fortov@ihed.ras.ru

Keywords: X-ray and optical short pulse lasers, ablation, laser cavitations, laser nanospallation

Abstract. Short laser pulse from infrared to X-ray wavelength raises pressure in a thin surface layer. This pressurized layer decays acoustically into vacuum from the outer boundary of a target and into the bulk side of a target. The decay and corresponding expansion of matter of the pressurized layer produce tensile stress τ which stretches matter of this layer during acoustic decay time $t_s = d_T / c_s$, where d_T is thickness of the pressurized layer. Stress τ increases when absorbed energy F_{abs} increases. A spallation layer separates from a target if stress τ overcomes material strength τ_{str}. Simulations show that there is a molten layer with thickness $\sim d_T$, when an illumination is powerful enough to achieve the threshold condition $\tau = \tau_{str}$. Therefore nucleation of voids takes place in liquid. A spallation layer is located between a nucleation zone and vacuum boundary.
This layer does not separate shortly after nucleation. In our case the thickness d_T of the spallation layer and its inertia (proportional to mass per unit of surface) are so small that after nucleation the deceleration of a spallation layer continues. This means that the cavitation bubbles continue to exist rather long time after their appearance in a nucleation process and therefore their walls continue to resist to stretching through surface tension. In usual cases with much thicker spallation layer the contribution of the bubble deceleration into total value of deceleration of velocity is negligible in comparison with deceleration during the time interval when stretched matter keeps it continuity.
Near threshold $\tau = \tau_{str}$ the resisting stage is so long in time that cooling due to heat conduction into cold bulk of a target freezes the bubbles. The undersurface bubbles, frozen jets with drops at the ends of jets, and remnants of walls of broken bubbles form random nanorelief at a target vacuum boundary. This conclusion follows from our recent experimental results and numerical simulations.

Introduction

Newton rings have been presented in paper [1]. This observation has begun studies of thermo-mechanical ablation. First explanation, why the interference rings appear, has been described in paper [2]. Let us introduce briefly physics of thermo-mechanical ablation. This will help better understand origin of surface nanostructures, since they are related to thermo-mechanical stretching of matter and fracture of spallation layer.

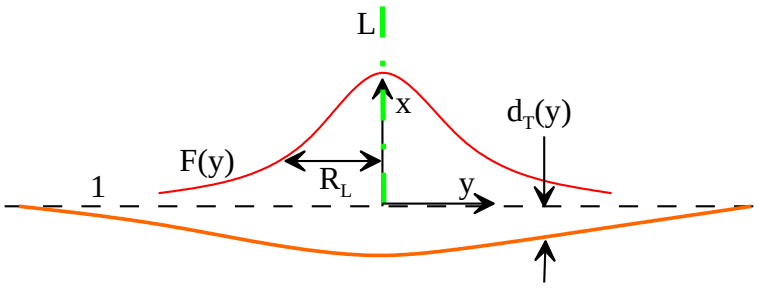

Fig. 1. Initial position of the target-vacuum boundary is the dashed line 1. Prior to a laser shot, target material was below the line 1; $F(y) = F_c \exp(-y^2 / R_L^2)$ is a fluence distribution around the axis L of a laser beam; d_T is thickness of a layer heated by laser.

Geometry of a target, its vacuum boundary, and a surface layer $d_T(y)$ heated by absorption of a laser pulse - all they are shown in Fig. 1. The heated layer in our experiments is shallow since its normal extension $d_T \sim 10-100$ nm is much smaller than its radial size defined by radius $R_L \sim 10-100$ microns of a laser beam. Laser pulse is short. Its duration is $\tau_L = 40$ fs – 10 ps. Laser

heating initiates expansion of the layer d_T shown in Fig. 1. At the ablation threshold F_{abl} voids nucleate at the nucleation depth $d_{crat}|_{abl}$, $d_{crat}|_{abl} \sim d_T$, see Fig. 2. Slightly above threshold F_{abl} radial extension $r_{nucl}|_{abl} = 0$ of the nucleation disk is small in comparison with beam radius R_L, see Fig. 2; the voids inside the disk are shown by circles. The nucleation disk is a spatial zone around beam axis L where nucleation of voids takes place. Near nucleation threshold, this disk is placed at the depth $d_{crat}|_{abl}$ under surface. The ablation threshold F_{abl} is higher than melting threshold. Therefore nucleation takes place in molten material. The curve m-c in Fig. 2 marks a front of melting and re-crystallization.

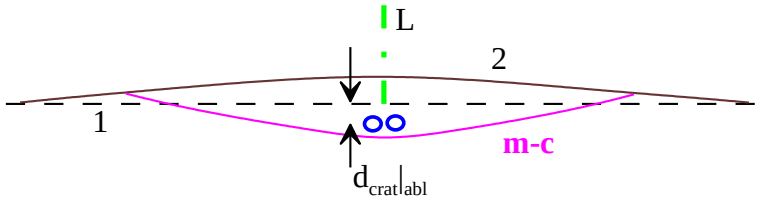

Fig. 2. Nucleation of voids inside of molten layer in case with fluence near threshold F_{abl}.

Due to expansion of heated matter, the vacuum boundary 1 in Figs. 1 and 2 moves in the normal direction x, compare current position 2 of the boundary with its initial position 1 in Fig. 2. Radial and normal extensions of a nucleation zone increase with fluence $F > F_{abl}$, see Fig. 3. Radial extension of nucleation zone is proportional to R_L if we fix relative central fluence $f_c = F_c / F_{abl}$. Normal extension increases when value f_c increases. In the shallow case $d_T << R_L$, normal extension does not depend on R_L. There is a definite value of fluence F_{ev} when a hole $d_{spall}(y=0) = 0$ in a spallation shell $d_{spall}(y)$ appears; $F_{ev} > F_{abl}$, see Fig. 3.

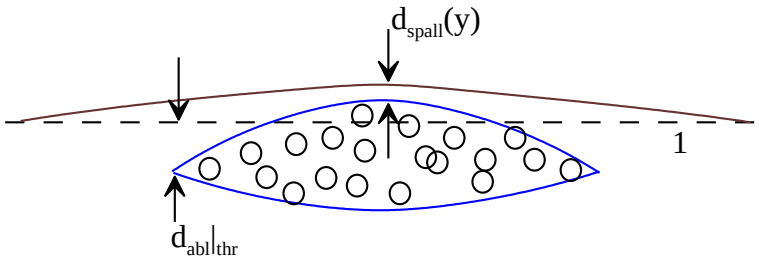

Fig. 3. Above ablation threshold the nucleation zone is the elongated volume with voids. The line 1 is initial boundary of target.

Figs. 1-3 describe principal features of the thermo-mechanical ablation. Ablation means removal of matter from target as a result of irradiation. In case of short pulse lasers the thermo-mechanical ablation gives dominant contribution into amount of removed mass. In this case a surface layer of mass is ablated by mechanical separation from target. This process is similar to spallation.

Undersurface frozen bubbles

Let $f_c = F_c / F_{abl}$ is slightly above 1 and radius R_L is large enough in comparison with depth d_T. In this situation the spallative run-away of the shell $d_{spall}(y)$ in Fig. 3 proceeds through decay of lateral walls between neighbor cavitation bubbles shown in Fig. 4 and coalescence of these bubbles into

large void which separates the shell $d_{spall}(y)$ from the rest of a target. After creation, the void increases in direction normal to the dashed line in Fig. 4 during run-away of the shell. The shell totally separates from a target in the region of lateral wall $r = y_{abl}$ shown in Fig. 4. Cavitation bubbles evolve inside a molten layer which gradually cools and freezes during and after the process of shell separation. The bubbles near the crater wall have a chance to keep frozen if cooling process is fast enough to leave behind the contraction and collapse of bubbles under action of surface tension. Bubbles near walls are shown in Fig. 4 (right). The two processes one of bubble inflation and second of bubble contraction compete with each other. Inflation of bubbles takes place during deceleration of the spallation shell [3-5]. Surface tension resists to the run-away of a shell and maintains deceleration of a shell. Surface tension begins to work for bubble contraction after separation of the spallation shell.

Fig. 4. Process of caviation and spallation: multiple nucleation in the elongated horizontal layer under the spallation shell $d_{spall}(y)$ shown in Fig. 3 (left); merging of small bubbles in the central region into the large void shown by oblate ellipsoid (left); run-away of the spallation shell $d_{spall}(y)$ and formation of the crater with sharp lateral walls (right); the walls correspond to the circle $r = y_{abl}$ where fluence achieves threshold $F_c \exp(-y_{abl}^2 / R_L^2) = F_{abl}$ (right); dashed line is an initial boundary.

A spallation shell is a cover above a cavitation zone in Fig. 3 or above an oblate void in Fig. 4. If absorbed fluence is above threshold $f_c = F_c / F_{abl} > 1$ then the cover runs-away. The run-away opens a central void and transforms a closed void into well. The well is a crater. Matter, which has filled the well, constitutes the shell. The rim around the lateral wall corresponds to a near-threshold region $F(y) \approx F_{abl}$. Small voids near the lateral wall in Fig. 4 may blow out, or remain frozen, or collapse and disappear. The broken small bubble "g" together with frozen one "h" is shown in Fig. 5. They locate inside the rim. If "g" is a broken small void, then "a" is a broken large void shown as an oblate ellipsoid in Fig. 4 (left).

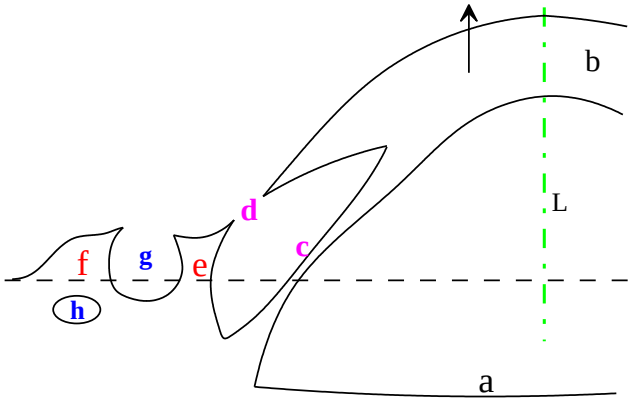

Fig. 5. Breaking of bonds "c" and "d" connecting the spallation shell "b" and a target. The circle of the lateral wall is the place of connection. The shell runs-away in normal direction shown by the arrow. The bonds decelerate runaway motion. The "e", "f" is an elevated rim around a wall. The rim is elevated above initial boundary shown by dashed line; "a" is a bottom of crater.

An image of topography of a laser crater on aluminum surface is shown in Fig. 6. This image has been obtained by focused ion beam (FIB) operating in low current regime. Ion beam produces secondary electrons collected by imaging system of an electron microscope. FIB in low current regime rival the more familiar scanning electron microscope (SEM) in terms of imaging topography. Fig. 6 presents a frontal view along the axis L normal to a plane of initial boundary, see Figs. 1, 2, and 5. Cr:forsterite laser pulse parameters for this shot are: duration100 fs, wavelength 1240 nm, 45^{o} is angle of incidence, $R_L = 25$ microns, $f_c = 1.05$. FIB image in Fig. 6 clearly shows details of an irradiated spot: the crater, the lateral wall of a crater, and the rim around the wall. This is a final image obtained much later after termination of all processes initiated by laser shot. The spallation shell, which covers the crater, has run-away. The inner rim connected with lateral wall is the place where separation of the cover from target has took place; see Fig. 5 which illustrates fracture of bonds between the shell and the target. The main rim, located outside to the wall, experienced near threshold irradiation but has kept connection with a target. Surface structures in the rim and at the bottom of crater are obviously different.

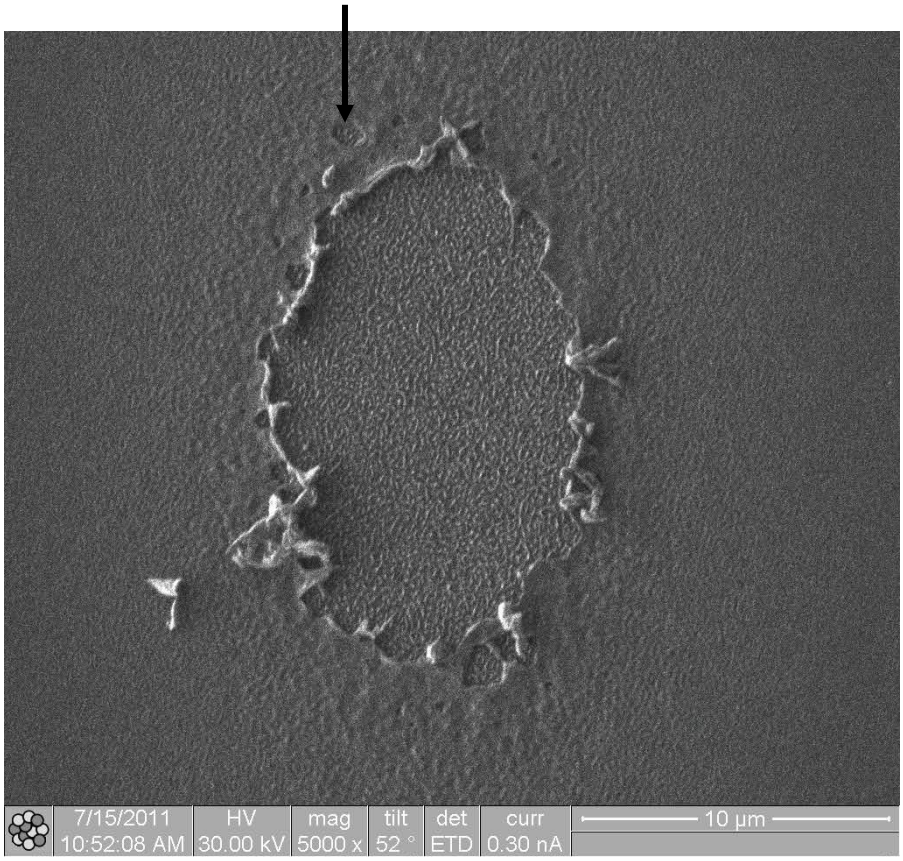

Fig. 6. Crater, near wall ellipse, and rim produced by a single laser shot.

There are traces of broken small bubbles in the rim. One of them is marked by arrow in Fig. 6. As was said above, the spallation shell covers association of small bubbles, while the arrow in Fig. 6 marks small crater corresponding to the individual small cavitation bubble similar to the broken bubble “g” in Fig. 5. The relief of surface in the rim has traces of knobs. It is suspicious that this relief hides frozen nanobubbles like bubble “h” shown in Fig. 5.

FIB image reveals fine details of structures created by laser pulse. This is important advantage. While great advantage of micro-interferometric technique is ability to measure the depths of extremely shallow structures, see profile of the crater in Fig. 7. Technique, used to obtain micro-interferometric image shown in Fig. 7, is described in paper [5], see also references in this paper.

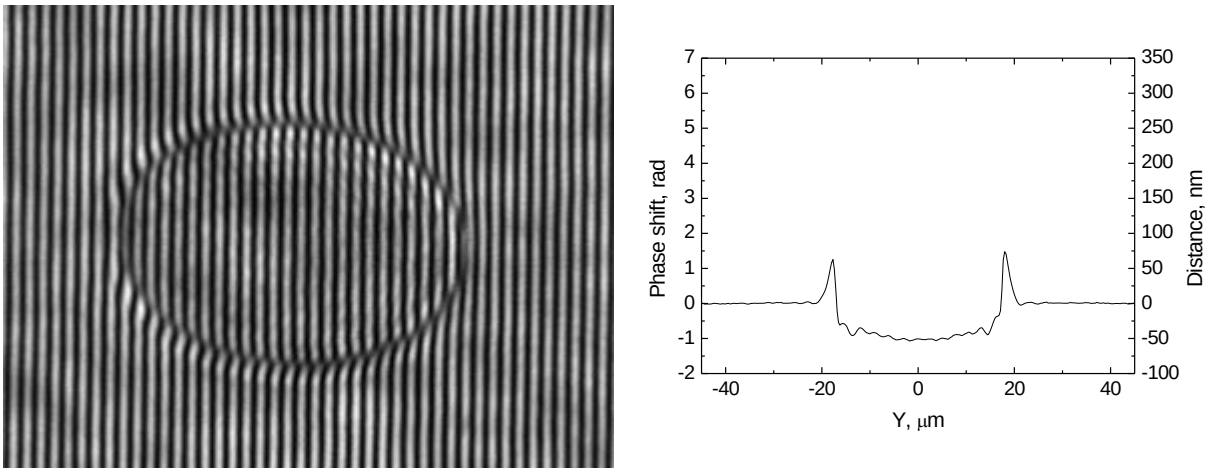

Fig. 7. Left: final micro-interferometric image of crater and rim around. Right: final profile of crater and rim at an aluminum target obtained from the micro-interferometric image shown in the left panel. These image and profile correspond to the crater shown in Fig. 6.

As was said above, region of the rim in Fig. 6 is suspicious. It may contain nanobubbles hidden under target boundary. To check this suggestion, we use combination of focused ion beam (FIB) and transmission electron microscopy (TEM) (Lamella technique [6,7]). A thin slice, crossing the crater wall and rim shown in Figs. 6 and 7, was, first, covered by protective layer of platinum metal-organic and, second, was cut from aluminum film. The slice crosses the rim in radial direction. The metal-organic layer protects surface structure, covered by the metal-organic layer, from ion milling. Target shown in Figs. 6 and 7 is an aluminum film deposited onto glass plate. The obtained slice has been separated from glass plate and has been transferred to TEM.

The TEM image of the obtained slice is shown in Fig. 8. In Fig. 8 the dark granulated layer on the top of Al surface is the platinum protective layer. We see that the nanobubbles form a layer under Al surface. The bubble layer thickness is 50-100 nm.

Frozen broken foam in the bottom of a crater

Ultrashort laser pulses (ULP) produce thermo-mechanical (TM) stress at an acoustical time scale. Such stresses are the reason for creation of frozen nano-bubbles (if $F \approx F_{abl}$, Fig. 8) and frozen disrupted foam ($F > F_{abl}$, Figs. 9,10). Results of irradiation by optical and X-ray ULP are similar in terms of production of TM stress, while the physics of light absorption varies qualitatively. Therefore optical and X-ray ULP both generate nano-deformed structures with frozen bubbles and foam.

Let us consider the case above threshold $F > F_{abl}$. There are multiple nucleations in a spatially extended region. New and new layers of cavitation bubbles are created as a stretching wave penetrates deeper into target. Formation of an ensemble of cavitation bubbles is accompanied by stretching of this ensemble due to inertial expansion of two-phase (vapor-liquid) mixture. The

stretching gradually decreases the volume fraction of liquid V_{liq}/V in the two-phase mixture. During stretching, the mixture evolves from (A) small bubbles in molten matter at small values of fraction V_{liq}/V to (B) the foam state at $V_{liq}/V \cong 1$ and >1. Finally at the stage (C) an expanding cloud of liquid droplets in vapor forms when $V_{liq}/V >> 1$.

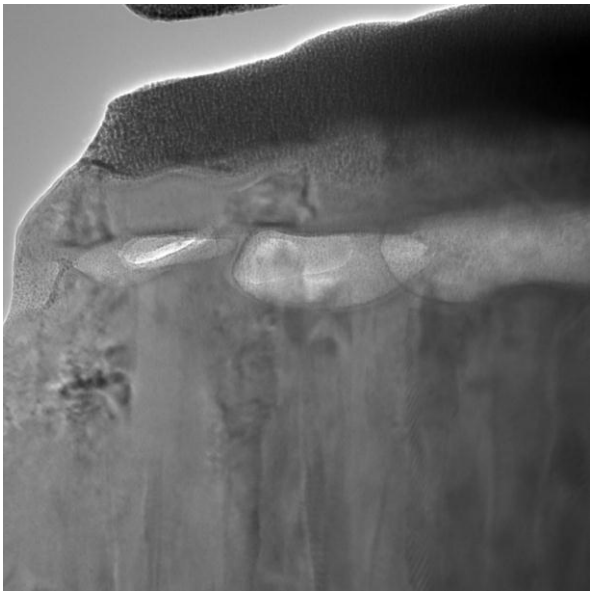

Fig. 8. The TEM image of a thin slice milled by FIB. The image reveals existence of frozen bubbles beneath the surface of Al film in the rim around the crater. The rim belongs to near-threshold region.

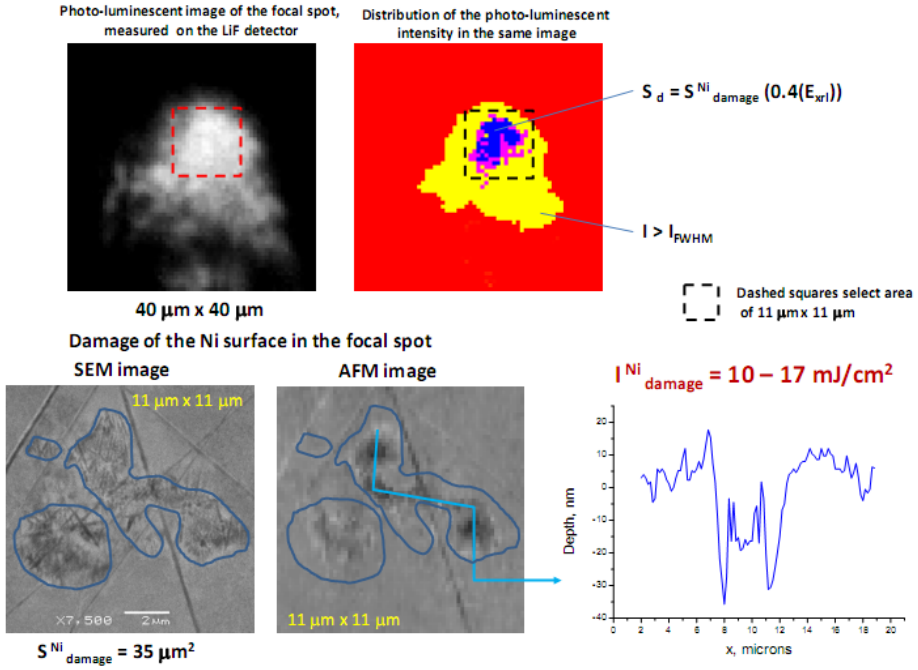

Fig. 9. Photo-luminescent (PL) image obtained at Lithium Fluoride (LiF) crystal; distribution of intensity according to the PL image; SEM image; AFM image; and the AFM damage profile, showing ablated depth inside the irradiated spot.

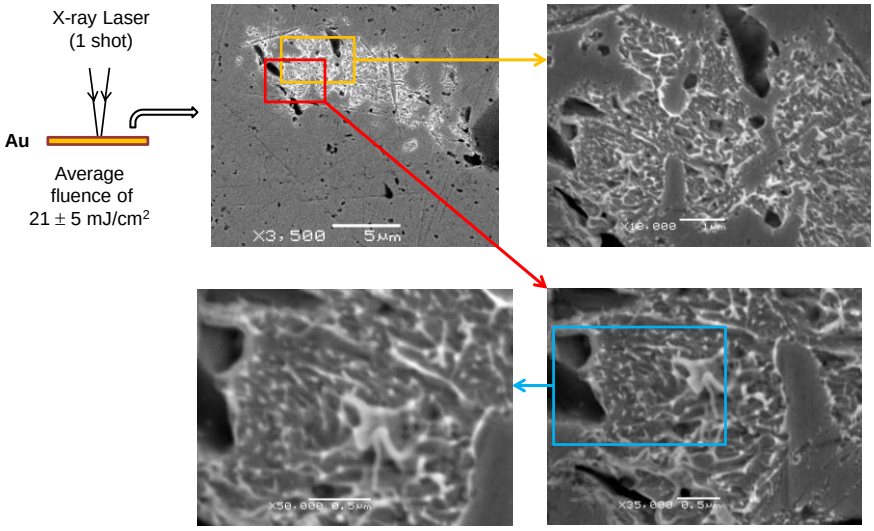

Fig. 10. Clear evidence of existence of frozen nano-foam structures after single X-ray shot.

There are the A,B,C stages listed above. Transition between the stages B and C from isolated bubbles to isolated droplets is carried out by gradual rupture of walls surrounding the inflated bubbles. It is gradual in the sense that the rupture of walls in the upper layer of bubbles takes place first. After that the next, deeper layer of walls decays. The up and down directions are as in Figs. 1-5 where the axis x is shown. As time progresses, the more and more deep layers of walls decay. There is a "front" of the decays propagating from the outer surface into the bulk of a target. Above the front there is percolation through vapor in the two-phase mixture, while below the front there is percolation through liquid.

Gradually the front of ruptures comes near and near to the bottom of the future crater. There are two converging fronts: the front of decays of liquid walls coming from the outer surface and the recrystallization front (see Fig. 2) separating melt and poly-crystal. The latter front moves up along the axis x from the side of bulk target.

X-ray pictures on Nickel (Fig. 9) and gold (Fig. 10) have been obtained at Ag plasma laser [8-14]. Intensity distributions are rather stable from shot to shot. Luminescence of color centers of irradiated LiF [8] has been used to define intensity distribution across the irradiated spot, see the upper left corner in Fig. 9. Qualitative reasons for appearance of frozen structures now are well established [8-10]. At the same time, there is still unclear why threshold on absorbed energy in the X-ray case is significantly below than the threshold in case of optical lasers acting on absorbing targets (in case considered here, there are metals), see the bottom right corner of Fig. 9 where threshold for Nickel is 10-17 mJ/cm^2, while for optical irradiation of Nikel the absorbed fluence at the ablation threshold is 140 mJ/cm^2 [15].

Summary

The main goal of this paper is to emphasize that the frozen nano-structures created by short pulse optical and X-ray lasers are similar. These structures are linked to thermo-mechanical stress and to

creation of pressurized surface layers existing during acoustic time scale near irradiated surface. Theory of the thermo-mechanical ablation by X-ray short pulse has been developed in papers [8-10].

Authors (NAI, SIAsh, YuVP, VAK, SIAn, MBA) acknowledge support from RFBR grant No. 10-02-00434-a

References

[1] K. Sokolowski-Tinten, J. Bialkowski, A. Cavalleri, D. von der Linde, A. Oparin, J. Meyer-ter-Vehn, and S.I. Anisimov: Phys. Rev. Lett. Vol. 81 (1998), p. 224

[2] N.A. Inogamov, Yu.V. Petrov, S.I. Anisimov, A.M. Oparin, N.V. Shaposhnikov, D. von der Linde, and J. Meyer-ter-Vehn: JETP Lett. Vol. 69(4) (1999), p. 310

[3] V. Zhakhovskii, N. Inogamov, K. Nishihara: J. Phys.: Conf. Ser. Vol. 112 (2008), 042080

[4] V.V. Zhakhovskii, N.A. Inogamov, K. Nishihara: JETP Lett. Vol. 87(8) (2008), p. 423

[5] S.I. Ashitkov, N.A. Inogamov, V.V. Zhakhovsky, Yu.N. Emirov, M.B. Agranat, I.I. Oleinik, S.I. Anisimov, and V.E. Fortov: JETP Lett. Vol. 95(4) (2012), p. 176

[6] L. Giannuzzi, F.A. Stevie: Eds., *Introduction to Focused Ion Beams: Instrumentation, Theory, Techniques and Practice* (Springer 2005)

[7] J. Mayers, L. Gianuzzi, T. Kamino, J. Michael: MRS bulettin Vol. 32(5) (2007), p. 400

[8] A.Ya. Faenov, N.A. Inogamov, V.V. Zhakhovskii, V.A. Khokhlov, K. Nishihara, Y. Kato, M. Tanaka, T.A. Pikuz, M. Kishimoto, M. Ishino, M. Nishikino, T. Nakamura, Y. Fukuda, S.V. Bulanov, T. Kawachi: Appl. Phys. Lett. Vol. 94 (2009), 231107

[9] N.A. Inogamov, A.Ya. Faenov, V.A. Khokhlov, V.V. Zhakhovskii, Yu.V. Petrov, I.Yu. Skobelev, K. Nishihara, Y. Kato, M. Tanaka, T.A. Pikuz, M. Kishimoto, M. Ishino, M. Nishikino, Y. Fukuda, S.V. Bulanov, T. Kawachi, S.I. Anisimov, V.E. Fortov: Contrib. Plasma Phys. Vol. 49(7-8) (2009), p. 455

[10] N.A. Inogamov, V.V. Zhakhovsky, A.Y. Faenov, V.A. Khokhlov, V.V. Shepelev, I.Y. Skobelev, Y. Kato, M. Tanaka, T.A. Pikuz, M. Kishimoto, M. Ishino, M. Nishikino, Y. Fukuda, S.V. Bulanov, T. Kawachi, Y.V. Petrov, S.I. Anisimov, V.E. Fortov: Appl. Phys. A Vol. 101(1) (2010), p. 87; arXiv:0912.3184

[11] M. Ishino, A.Ya. Faenov, M. Tanaka, N. Hasegawa, M. Nishikino, S. Tamotsu, T.A. Pikuz, N.A. Inogamov, V.V. Zhakhovsky, I.Yu. Skobelev, V.E. Fortov, V.A. Khohlov, V.V. Shepelev, T. Ohba, T. Kaihori, Y. Ochi, T. Imazono, T. Kawachi: J. Appl. Phys. Vol. 109 (2011), 013504

[12] N.A. Inogamov, A.Ya. Faenov, V.V. Zhakhovskii, I.Yu. Skobelev, V.A. Khokhlov, Y. Kato, M. Tanaka, T.A. Pikuz, M. Kishimoto, M. Ishino, M. Nishikino, Y. Fukuda, S.V. Bulanov, T. Kawachi, Yu.V. Petrov, S.I. Anisimov, V.E. Fortov: Contrib. Plasma Phys. Vol. 51(4) (2011), p. 361

[13] N.A. Inogamov, A.Ya. Faenov, V.V. Zhakhovsky, T.A. Pikuz, I.Yu. Skobelev, Yu.V. Petrov, V.A. Khokhlov, V.V. Shepelev, S.I. Anisimov, V.E. Fortov, Y. Fukuda,M. Kando, T.Kawachi, M. Nagasono, H. Ohashi, M. Yabashi, K. Tono, Y. Senda,T. Togashi, and T. Ishikawa: Contrib. Plasma Phys. Vol. 51(5) (2011), 419

[14] N.A. Inogamov, S.I. Anisimov, V.V. Zhakhovsky, A.Ya. Faenov, Yu.V. Petrov, V.A. Khokhlov, V.E. Fortov, M.B. Agranat, S.I. Ashitkov, P.S. Komarov, I.Yu. Skobelev, Y. Kato, T.A. Pikuz, V.V. Shepelev, Y. Fukuda, M. Tanaka, M. Kishimoto, M. Ishino, M. Nishikino, M. Kando, T. Kawachi, M. Nagasono, H. Ohashi, M. Yabashi, K. Tono, Y. Senda, T. Togashi, T. Ishikawa: Proc. SPIE, 7996, 79960T (2011)

[15] N.A. Inogamov, Yu.V. Petrov, V.V. Zhakhovsky et al: Santa-Fe, HPLA-2012 Proc. (accepted).